Progress in Propulsion Physics **4** (2013) 257-270
DOI: 10.1051/eucass/201304257

EXPERIMENTAL INVESTIGATION OF ISOLATED ACETONE DROPLETS AT AMBIENT AND NEAR-CRITICAL CONDITIONS, INJECTED IN A NITROGEN ATMOSPHERE

E. Oldenhof[1], F. Weckenmann[1], G. Lamanna[1], B. Weigand[1], B. Bork[2], and A. Dreizler[2]

[1]Institut für Thermodynamik der Luft- und Raumfahrt
Universität Stuttgart
Pfaffenwaldring 31, 70569 Stuttgart, Germany

[2]FG Reaktive Strömungen und Messtechnik, Maschinenbau
Center of Smart Interfaces, TU Darmstadt
Petersenstraße 32, Darmstadt 64287, Germany

A new experimental setup is presented to investigate free falling acetone droplets at ambient to near-critical temperatures, injected in a heated and pressurized nitrogen atmosphere. Important considerations for the design are: a high reproducibility of the experiments, control of the temperature of the generated droplet independent from that of the chamber, and the homogeneity of the surroundings. In the reported experiments, chamber temperatures range from 293 to 523 K, chamber pressures from 1 to 60 bar and acetone injection temperatures from 293 to 466 K. The reproducibility of all experiments is found to be excellent when the chamber temperature is low (318 K or less). The droplet diameters under these circumstances are reproducible within 1%, even at the highest pressure of 60 bar. The droplet detachment time relatively to the external trigger is also very reproducible, within 0.5 ms. At higher chamber temperatures, the droplets are more sensitive to disturbances, but can still be created "on-demand." The novel experimental setup is thus capable of generating reliable and comparable experiments at high pressures and temperatures up to supercritical chamber conditions.

1 INTRODUCTION

Supercritical fluids are found in a very wide range of industrial applications. The capabilities of supercritical fluids for extraction purposes have been recognized

for over decades, whereas more recent developments are the use of supercritical CO_2 in synthesis processes [1] or in heat pumps to achieve high thermodynamic efficiencies [2].

Supercritical phenomena are also relevant to devices where liquids are injected in an environment with supercritical properties with respect to the liquid, as occurs in Diesel engines, gas turbines or in rocket engines where cryogenic oxygen is injected [3]. In these situations, a large number of complex physical phenomena occur. Initially, the injected fluid is a liquid (having a certain surface tension and heat of evaporation). However, due to mixing and diffusion processes, the liquid might turn into a supercritical fluid with distinctly different properties. Here, a central issue is how fast the transcritical jet breaks up and mixes with its surroundings, making the reactants available.

The thermodynamic anomalies associated with the critical point provide great difficulties when near-critical behavior is to be modeled or analyzed [4]. The invalidity of the commonly employed ideal gas assumptions with respect to transport properties, the high solubilities, the strong changes (e. g., in c_p and c_v) that occur around the critical point, and the compressibility of near-critical fluids make the simulation of practical situations, such as an entire spray injected at supercritical surroundings, very challenging. Experiments are therefore crucial to deepen the understanding and to enable the development of more realistic models.

It has been recognized in several studies that the phenomena in transcritical jets are distinctly different from those in subcritical jets. The experiments by Oschwald *et al.* [5] show these differences, perhaps, most clearly. In one of their experiments, liquid nitrogen was injected at subcritical temperature ($T \approx 110$ K, whereas $T_c(N_2) = 126$ K) into a chamber filled with nitrogen at supercritical temperature (300 K), varying the chamber pressure from a sub- to supercritical value. A qualitative change in the jet morphology was shown: whereas the subcritical spray exhibited the characteristics of atomization, the transcritical spray showed no sign of the presence of droplets. Instead, diffusive finger-like structures were seen. In accordance with the more gas-like behavior at supercritical conditions, the fractal dimension of the interface at these conditions was shown to assume a value close to that measured in gaseous jets.

At the fundamental level, understanding of the processes occurring in a single droplet is a premise to the understanding of the more complex case of an entire spray. Experiments on suspended droplets have been performed for several decades, either in microgravity or normal gravity, in quiescent surroundings or moving air [6–9]. This arrangement precludes the study of droplets that approaches the supercritical mixing state, as surface tension is needed to suspend the droplet.

Also, the effect of the fibre is nonnegligible to the evaporation process [4]. The numerical modeling of single droplets in near-critical conditions still has the status of work in progress [4], even in the most idealized conditions (micro-

gravity, quiscent surroundings). Therefore, most of the works have been focused on the study of droplets in the idealized case of a stagnant surroundings with no gravitation [10, 11]. Considering this state of numerical modeling, it may be desirable to have the availability of experiments that approach such idealized conditions as much as possible.

On the other hand, free falling droplets in normal gravity are more relevant for a realistic spray, being subjective to a convective atmosphere. Additionally, the limitation of only being able to study fluid which is well below the critical temperature — as in suspended droplet studies — is overcome when studying free falling droplets. Stengele *et al.* [12] developed a setup to create and detach droplets on demand and studied free falling one- and two component pentane and nonane droplets in a nitrogen atmosphere. The chamber could be heated and pressurized to supercritical conditions with respect to the liquid. The droplet size and velocity as a function of the fall distance was reported, for varying the initial droplet size, the chamber pressure, and the temperature. A supercritical mixing state was not reached in the experiments, probably, because the droplets were injected at relatively low temperatures (between 370 and 380 K).

In this paper, the development and the first results of the measurement setup that generates single drops, injected at ambient to near-critical temperatures and ambient to supercritical pressures are described. These experiments can be subdivided in two categories, namely, those carried out with an unheated chamber and those carried out with the heated chamber.

2 EXPERIMENTAL SETUP

2.1 Pressure Chamber

The experimental setup consists of an optically accessible and heatable high-pressure chamber, which has a droplet generator mounted inside (Fig. 1*a*). The main housing is made of a single block of highly resistant steel 1.4571 and has four ultraviolet transparent quartz windows for optical accessibility. The external view is provided in Fig. 1*b*. The chamber has been pressure tested up to 85 bar.

The chamber is heated with six heating cartridges: four vertically mounted cartridges heating most of the length of the chamber, and two horizontally mounted cartridges at the bottom. Several T-type thermocouples are installed in the chamber wall to monitor the steel temperature, and inside the chamber, to measure the nitrogen temperature. The pressure is measured with a digital temperature-compensated Keller PAA-35XHTC pressure transducer that has an accuracy of ± 300 mbar between 0 and 60 bar. Both the temperature

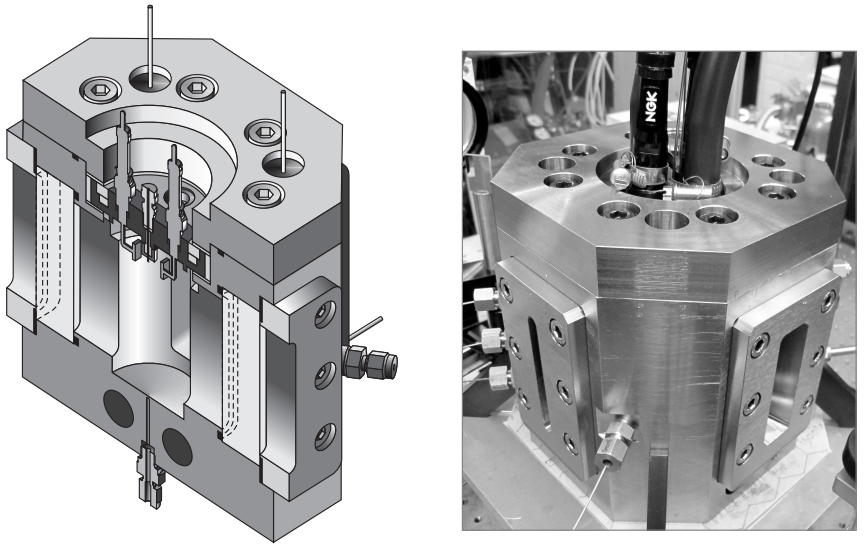

(*a*) (*b*)

Figure 1 Experimental setup: a three-dimensional view of the interior of the setup (*a*); and exterior view of the setup (*b*)

and the pressure are monitored continuously (at 10 and 100 Hz, respectively). A Bronkhorst Mini-Coriflow mass flow controller measures and controls the acetone supply. The acetone comes from a pressure vessel that is held at a pressure of about 5 bar higher than that of the chamber and is pressurized with helium. Helium is chosen because of its low solubility, to prevent bubble formation at the capillary (which was observed previously when nitrogen was used as pressurization gas).

Solenoid valves are mounted in the fluid supply system, to fill and empty the chamber to the required pressure. The solenoid valves are operated by an in-house routine written in Labview that, based on the pressure reading, opens and shuts off valves as required. The start-up procedure consists of filling the chamber until a certain pressure level so that the desired pressure level is slightly exceeded after the subsequent heating of the chamber, and, finally, releasing some gas to exactly reach the desired pressure.

2.2 Droplet Generator

A big challenge of the setup is to create droplets in a near- or supercritical environment with a temperature not far below the critical temperature (0.7

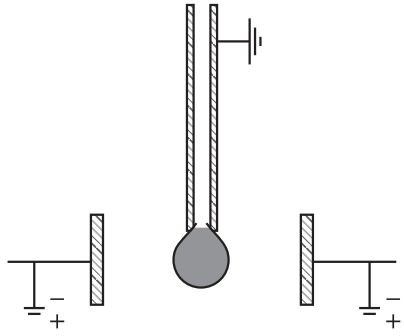

Figure 2 Schematic of the developed eletric droplet detachment system. The steel capillary is grounded, the electrodes can be charged with up to 10 kV, during time intervals ranging from milliseconds to several seconds

$< T/T_c < 0.95$). With the reduced surface tension under these conditions, standard droplet generators cannot be used, as they become increasingly unstable at higher temperatures. To still have the ability to control the detachment process and to generate well defined droplets, a technique has been developed whereby an external electric field is shortly imposed on the droplet, to trigger the detachment process. The basic physical principle of this technique is that the charge distribution within the droplet is influenced by the external electric field, which decreases the effective surface tension and produces an external electric force [13].

The schematic of the system is shown in Fig. 2. Note that the capillary is grounded and the electrodes are placed symmetrically around the capillary to prevent any lateral deflection of the droplet. During operation, a particular care is taken to make sure that the droplet is not charged upon detachment. This is achieved by applying a very short electric pulse just to destabilize the drop from its mechanical equilibrium state. During the actual detachment, the electrical field is turned off and the residual surface charge is rapidly discharged through the grounded capillary.

Because of the high evaporation rates, filling the droplet until the desired size is not a trivial task. To be able to trigger the electric field at the right instant, a laser-optical detection system was built. A lens focuses a low-intensity (1 mW) laser beam below the capillary so that the beam is broken when the droplet has the desired size. The change in light intensity is detected by a fast photo diode, whose signal is transformed to a TTL (transistor–transistor logic) signal, upon which a timing unit (Labsmith LC880) triggers the high voltage power supply to detach the droplet. The thickness of the laser beam at its waist is measured to be approximately 20 μm. The high-voltage feed-through system is realized by the use of spark plugs (NGK DCPR-6 E). Copper

electrodes are mounted on the center electrode, and installed on both sides of the capillary. The electrodes are cast in a highly temperature resilient epoxy-based glue (Duralco 4700 HT) to prevent an electric breakdown of the surrounding atmosphere. With this design, electric fields up to 10 kV can be created inside the chamber. The capillary has the inner diameter of 200 μm and the outer diameter of 700 μm.

The injector is heated independently of the chamber by a recirculating oil system. Isolation material attached to the top of the injector prevents a large heat flux from the chamber to the injector and reduces unwanted recirculations associated with convective heat transfer. The injector can be heated up to 473 K, which is 93% of the critical temperature of acetone. Reported injector temperatures are measured with a T-type thermocouple inside the injector, as close as possible to the capillary, at the radial distance of approximately 5 mm.

2.3 Optical Setup

The imaging system consisted of a Photron SA-1 high speed camera equipped with an Infinity K2/SC long-distance microscope. The spatial resolution at the used distance was 13 μm per pixel. The camera was operated at 2000 frames per second. Uniform back lighting was achieved by collimating the light of a high-power LED (Lumeon Rebel) with a lens. The post-processing consisted of applying a threshold-based boundary detection to describe the contour of the droplet, from which quantities such as the size and velocity of the droplet were derived. In the measurements on the unheated chamber, the visual border between the droplets and the background is very sharp. Because of this high contrast, a range of thresholds can be chosen without influence on the droplet contour. The determination of the projected droplet boundary therefore involves little arbitrariness. With the droplets in the heated chamber, the stronger evaporation results in dark structures surrounding the droplet, which prevents an accurate determination of the droplet size from the shadowgraphy images.

2.4 Operational Parameters

An extensive test series was carried out to investigate the performance of the injector under a wide range of conditions. Acetone, which has a critical temperature $T_c = 508$ K and a critical pressure $p_c = 48$ bar, was used as the working fluid. The chamber atmosphere was nitrogen. The chamber temperature was varied, between 293 K and 523 K (which corresponds to the reduced temperature T_{ch}/T_c of 1.03), with the critical properties of acetone as a refer-

Table 1 Matrix of the experimental conditions. T_{inj} indicates the temperature of the injector, T_{ch} and p_{ch} indicate the temperature and pressure of the nitrogen inside the chamber, respectively. The saturation pressure of pure acetone (p_{sat}) is included as a reference. This pressure is calculated with the PR-EOS for acetone, with parameters taken from [14]

	Unheated chamber			Heated chamber	
T_{ch}, K	293	298	318	376	523
T_{inj}, K	293	373	423	377	466
p_{sat}, bar	0.240	3.70	11.5	4.10	24.9
p_{ch}, bar					
1.0	X				
20	X				
40	X	X	X		
50					X
60	X			X	

ence. Chamber pressures up to 60 bar ($p_{\mathrm{ch}}/p_c = 1.2$) and injector temperatures up to 466 K ($T_{\mathrm{inj}}/T_c = 0.92$) were used. The droplets were detached with the voltage of 2.0 kV, and the pulse duration of 10 ms. Each test point comprised three different experiments. Evidently, no experiments were conducted at pressures below the vapor pressure, which is why the test matrix does not contain points of low pressure at high temperatures. The complete test matrix is depicted in Table 1. The experiments are divided into those at which the chamber is unheated, and those with the heated chamber. Note that the chamber heats up slightly when the injector is heated due to the imperfect thermal isolation.

2.5 Thermodynamic Properties of Nitrogen–Acetone Mixtures

The temperatures and pressures are related in this paper to the critical values of acetone, which is relevant for the liquid inside the droplet. In the mixing region close to the droplet and in the edge of the droplet, however, the properties of mixtures of acetone and nitrogen are important. Prof. Vrabec from the University of Paderborn kindly provided this data, which was obtained numerically using a Peng–Robinson equation of state (PR-EOS) and the quadratic mixing rule. The parameters for the PR-EOS were validated experimentally by Windmann *et al.* [14]. It has to be noted that close to the critical point, the accuracy resulting from the PR-EOS is not always guaranteed; nevertheless, it provides a good estimate [15].

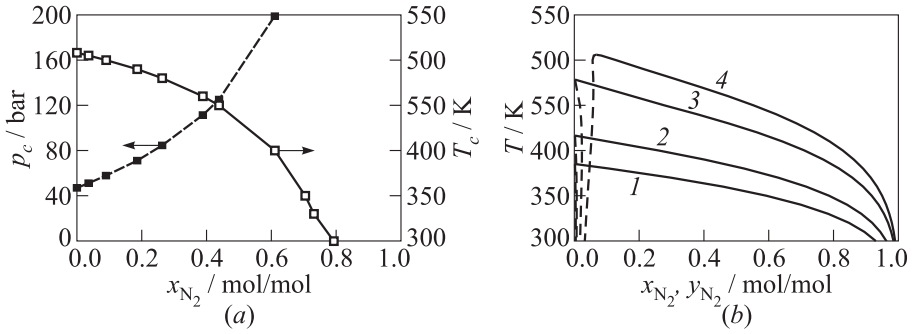

Figure 3 Thermodynamic properties of the acetone/nitrogen mixture, obtained numerically from the PR-EOS, with parameters from [14]: (*a*) critical pressure and temperature; and (*b*) phase separation lines at several pressures (*1* — 5 bar; *2* — 10; *3* — 30; and *4* — 60 bar)

Figure 3*a* shows the critical pressure and temperature of mixtures of acetone and nitrogen. Starting from pure acetone, an increase in the mole fraction of nitrogen is seen to be accompanied by a strong increase of the critical pressure of the mixture, whereas the critical temperature goes down. The supercritical mixing state is therefore most likely not reached outside of the droplet.

Figure 3*b* shows the phase separation lines at several pressures. The solid lines indicate the transition from the vapor phase to the two-phase regime, while the dashed lines indicate the transition from the liquid to the two-phase regime.

3 RESULTS

3.1 Visual Observations

An impression of droplets generated at distinctly different conditions is provided in Fig. 4. The droplet shown in Fig. 4*a* (generated at 1 bar pressure, room temperature) is the largest of the three. The droplet shown in Fig. 4*b* (also generated at room temperature, but at 60-bar pressure) is somewhat smaller. It has a faintly visible trailing vortical wake structure, likely related to the higher densities and density differences at these elevated pressures. The droplet in Fig. 4*c* is the smallest, and evaporates already strongly when detached. When falling, it generates visible streaks of acetone vapor.

The size of the formed droplets is related to the surface tension of the acetone. The focal point of the laser that triggers the recording is kept constant,

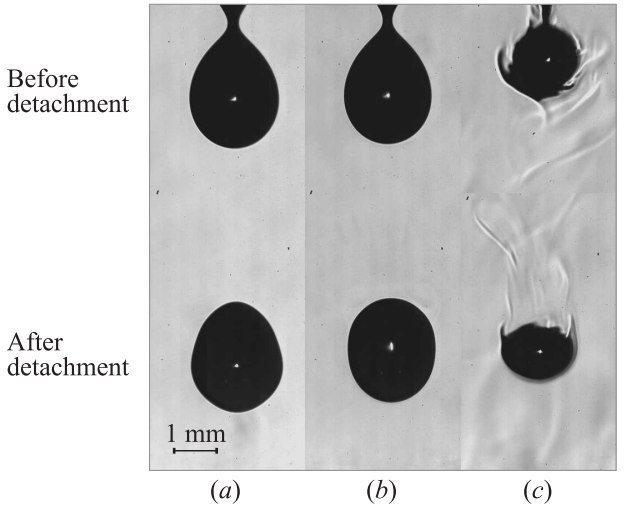

Figure 4 Three droplets generated at different conditions, with two snapshots of each. The snapshots correspond for all three images to 0.5 ms before and 28 ms after the droplet detachment: (*a*) $p_{ch} = 1$ bar, $T_{ch} = 293$ K, and $T_{inj} = 293$ K; (*b*) $p_{ch} = 60$ bar, $T_{ch} = 293$ K, and $T_{inj} = 293$ K; and (*c*) $p_{ch} = 50$ bar, $T_{ch} = 523$ K, and $T_{inj} = 466$ K

the bottom of the droplet is, therefore, always at a fixed distance from the capillary at the moment of triggering. As the surface tension is inversely proportional to the curvature of the drop, a large surface tension will result in a more spherical and voluminous droplet. The decreasing droplet size from the left to the right in Fig. 4 is, therefore, related to the decrease in surface tension.

3.2 Reproducibility

Droplet motion. The reproducibility of the droplet injector has been evaluated by producing several droplets under identical conditions. The images from three consecutive injections at ambient temperature and pressure, and at elevated pressure, are displayed in Fig. 5*a*. Note that the droplet boundary is sharp due to the image processing algorithm: only pixel values within the recognized droplet contour are displayed. A very good correspondence between the different realizations is seen, both in the timing of the detachment and the size and shape of the produced droplets.

At identical temperature but at higher pressure of 60 bar, the reproducibility is also very good (Fig. 5*b*). At high temperatures the behavior at the capillary becomes more chaotic. This is related to the simultaneous decrease in surface

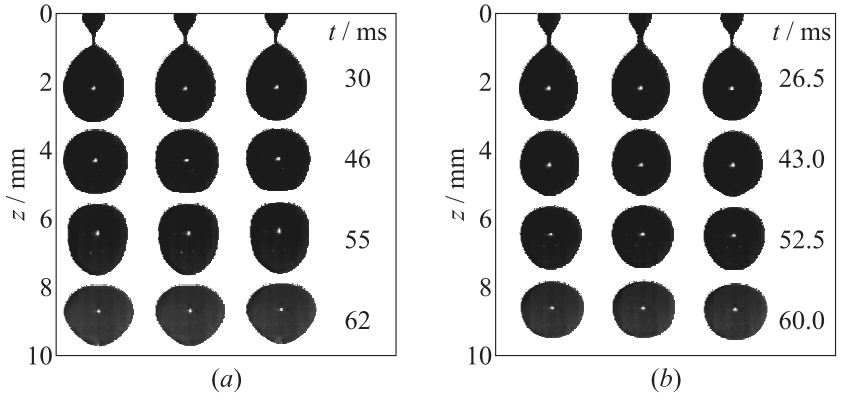

Figure 5 Snapshots from several droplet injections at ambient temperatures and the chamber pressure of 1 bar (a) and of 60 bar (b). The times shown are relative to the trigger signal. Droplet detachment takes place between the time of the upper snapshot and the following frame (i. e., within 0.5 ms); $T_{\rm ch} = 293$ K and $T_{\rm inj} = 293$ K

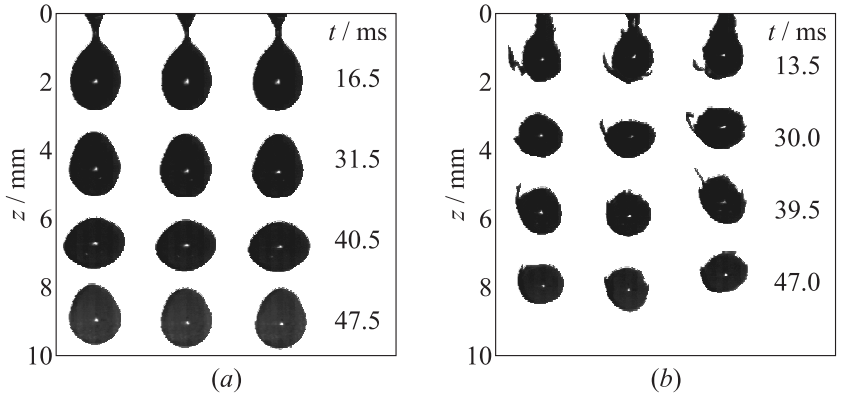

Figure 6 Snapshots from several droplet injections at elevated injector temperatures and chamber temperatures and pressures: (a) the injector and the chamber temperatures are approximately equal and subcritical ($p_{ch} = 60$ bar, $T_{ch} = 376$ K, $T_{\rm inj} = 377$ K, and $T_{\rm ch}/T_c$=0.74), and (b) the chamber temperature and pressure are just above critical ($p_{\rm ch} = 50$ bar, $T_{\rm ch} = 523$ K, $T_{\rm inj} = 466$ K, $T_{\rm ch}/T_c$=1.03, and $p_{\rm ch}/p_c$=1.04)

tension, and stronger effects of convection due to temperature differences between the chamber and the injector, leading to a worse reproducibility when events are related to the trigger time (Fig. 6a).

Droplet size. To give an indication of the size of the injected droplets, an effective diameter was estimated from the two-dimensional high speed shadowgraph images. This was only done with the experiments in the unheated chamber (see Table 1). A rotationally symmetric droplet shape was assumed (with the rotation axis parallel to the capillary), such that the volume of the body of revolution could be determined by integration in cylindrical coordinates. The effective droplet diameter was calculated according to a sphere with identical volume.

The evolution of the volume and equivalent droplet diameter are shown in Fig. 7. The curves of the different experiments are seen to lie very closely on each other. The sudden upward jump is related to the detachment (when the droplet is still attached, the droplet volume is not calculated). The curves are seen to fluctuate slightly, which is caused by the oscillation of the droplet. Given the large deformations of the droplets, the magnitude of the fluctuation in the calculated effective droplet diameter of less than 2% indicates that the assumption of axisymmetry is very reasonable.

In Fig. 8, average effective droplet diameters for different experimental conditions are shown. The averaging procedure (needed because of the slight fluctuations in time) consisted in determing the first minimum and maximum of the calculated diameter, and taking the arithmetic mean.

A minor decrease (of 4%) in droplet diameter is seen when the pressure is raised from 1 to 60 bar. A stronger effect is witnessed when the temperature of the injected acetone is raised from 293 to 423 K, the droplet diameter decreasing by 19%. This effect is related to the decrease in surface tension with rising temperature. The reproducibility in the droplet size is very good in all cases with the unheated chamber (deviations less than 1%).

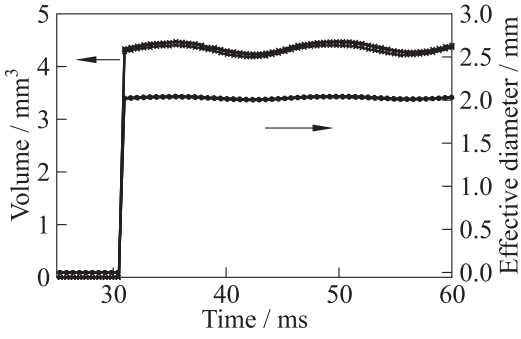

Figure 7 The droplet volume and effective diameter calculated by assuming axisymmetry, for three experiments at the pressure of 60 bar and the injector temperature of 293 K

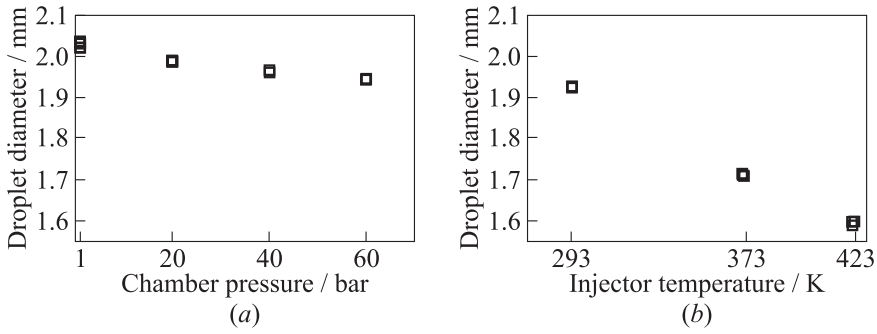

Figure 8 The effective diameter of the droplets formed by the injector as a function of chamber pressure, at the injector temperature of 293 K (a) and as a function of injector temperature, at the chamber pressure of 40 bar (b). The chamber was in all cases unheated. Note that, although not always visible due to the good reproducibility, each pressure/temperature combination comprises at least three measurement points

4 CONCLUDING REMARKS

A new experimental setup was developed to investigate free falling acetone droplets, injected in a nitrogen atmosphere. The optically accessible test chamber can be heated up to 525 K with the operational pressure of at most 60 bar, thus providing a supercritical environment with respect to the injected liquid, for liquids such as acetone and n-heptane. The injector that provides the liquid can also be heated, independently from the chamber, up to a temperature of 373 K. First experiments were performed with acetone droplets falling into a nitrogen environment, at different pressures and temperatures for both the injector and the chamber.

The appearance as well as the size of the droplets changed significantly with pressure and temperature. With the acetone temperature increasing, the size the droplets were found to strongly decrease, which can be explained by the lower surface tension of the liquid. The droplet size also decreased with the increasing pressure, albeit in a less pronounced manner.

The experiments showed a very good reproducibility for droplet injections with identical test conditions. The droplet diameter and time of detachment have, in unheated chamber conditions and up to 60 bar, a reproducibility error of less than 1% and 0.5 ms, respectively. When the chamber is additionally heated, the shadowgraph images show dark regions around the droplet, presumably of gaseous or supercritical acetone. This prevents an accurate determination of the droplet size. Judging from the visual data, the droplet detachment process is still fairly reproducible under near-critical conditions.

The evaporation processes in near-critical acetone droplets will be the focus of the next experimental campaigns. To gain also insight into the structures and processes inside the droplet during its fall, different optical measurement techniques like Mie scattering and laser-induced fluorescence will be applied.

ACKNOWLEDGMENTS

The authors greatly acknowledge the financial support by the DFG (Deutsche Forschungsgemeinschaft). Furthermore, the authors would like to thank Prof. J. Vrabec from the University of Paderborn for the useful discussions and the thermodynamic data, and Prof. Santini from the University of Bergamo for the fruitful suggestions during the development of the electric injection procedure.

REFERENCES

1. Cooper, A. I. 2000. Polymer synthesis and processing using supercritical carbon dioxide. *J. Mater. Chem.* 10(2):207–34.
2. Kim, M., J. Pettersen, and C. W. Bullard. 2004. Fundamental process and system design issues in CO_2 vapor compression systems. *Prog. Energy Combust. Sci.* 30(2):119–74.
3. Yang, V. 2000. Modeling of supercritical vaporization, mixing, and combustion processes in liquid-fueled propulsion systems. *Proc. Combust. Inst.* 28:925–42.
4. Bellan, J. 2000. Supercritical (and subcritical) fluid behavior and modeling: Drops, streams, shear and mixing layers, jets and sprays. *Prog. Energy Combust. Sci.* 26(4-6):329–66.
5. Oschwald, M., J. J. Smith, R. Branam, J. Hussong, A. Schik, B. Chehroudi, and D. Talley. 2006. Injection of fluids into supercritical environments. *Combust. Sci. Technol.* 178(1-3):49–100.
6. Savery, C. W., D. L. Juedes, and G. L. Borman. 1971. *N*-heptane, carbon dioxide, and chlorotrifluoromethane droplet vaporization measurements at supercritical pressures. *Ind. Eng. Chem. Fund.* 10(4):543–53.
7. Matlosz, R. L., S. Leipziger, and T. P. Torda. 1972. Investigation of liquid drop evaporation in a high temperature and high pressure environment. *Int. J. Heat Mass Transfer* 15(4):831–46; IN9:847–52.
8. Nomura, J., Y. Ujiie, H. J. Rath, J. Sato, and M. Kono. 1996. Experimental study on high-pressure droplet evaporation using microgravity conditions. *Symposium (International) on Combustion Proceedings* 26(1):1267–73.
9. Morin, C., C. Chauveau, P. Dagaut, I. Gokalp, and M. Cathonnet. 2004. Vaporization and oxidation of liquid fuel droplets at high temperature and high pressure: Application to *n*-alkanes and vegetable oil methyl esters rid a-4907-2010 rid c-1709-2008. *Combust. Sci. Technol.* 176(4):499–529.

10. Curtis, E. W., and P. V. Farrell. 1988. Droplet vaporization in a supercritical microgravity environment. *Acta Astronautica* 17(11-12):1189–93.
11. Haldenwang, P., C. Nicoli, and J. Daou. 1996. High pressure vaporization of LOx droplet crossing the critical conditions. *Int. J. Heat Mass Transfer* 39(16):3453–64.
12. Stengele, J., K. Prommersberger, M. Willmann, and S. Wittig. 1999. Experimental and theoretical study of one- and two-component droplet vaporization in a high pressure environment. *Int. J. Heat Mass Transfer* 42(14):2683–94.
13. Zhang, X. G., and O. A. Basaran. 1996. Dynamics of drop formation from a capillary in the presence of an electric field. *J. Fluid Mech.* 326:239–63.
14. Windmann, T., A. Köster, and J. Vrabec. Vapor–liquid equilibrium measurements of the binary mixtures nitrogen + acetone and oxygen + acetone. dx.doi.org/10.1021/je201058j.
15. Vrabec, J., Y. Huang, and H. Hasse. 2009. Molecular models for 267 binary mixtures validated by vapor–liquid equilibria: A systematic approach. *Fluid Phase Equilibria* 279(2):120–35.